

Air-Degradation Mechanisms in Mixed Lead-Tin Halide Perovskites for Solar Cells

Vincent J.-Y. Lim, Aleksander M. Ulatowski, Christina Kamaraki, Matthew T. Klug, Laura Miranda Perez, Michael B. Johnston, and Laura M. Herz*

Owing to the bandgap-bowing effect, mixed lead-tin halide perovskites provide ideal bandgaps for the bottom subcell of all-perovskite tandem photovoltaic devices that offer fundamentally elevated power-conversion efficiencies. However, these materials suffer from degradation in ambient air, which worsens their optoelectronic properties and hinders their usability for photovoltaic applications. Such degradation pathways are not yet fully understood, especially for the perovskites in the middle of the $\text{APb}_x\text{Sn}_{1-x}\text{I}_3$ solid solution line, which offer the narrowest bandgaps across the range. This study unravels the degradation mechanisms of $\text{APb}_x\text{Sn}_{1-x}\text{I}_3$ perovskites, reporting clear differences between mixed lead-tin ($x = 0.5$) and tin-only ($x = 0$) perovskites. The dynamic optoelectronic properties, electronic structure, crystal structure, and decomposition products of the perovskite thin films are examined in situ during air exposure. Both perovskite compositions suffer from the formation of defects over the timescale of hours, as indicated by a significant reduction in their charge-carrier diffusion lengths. For tin-only perovskite, degradation predominantly causes the formation of energetically shallow tin vacancies and hole doping. However, for mixed lead-tin perovskite, deep trap states are formed that significantly accelerate charge-carrier recombination, yet leave mobilities relatively unaffected. These findings highlight the need for passivation strategies tailored specifically to mixed lead-tin iodide perovskites.

1. Introduction

Metal-halide perovskites (MHPs) have gained much attention over the past decade,^[1–3] owing to their excellent properties, including high absorption coefficients,^[4] long charge-carrier diffusion lengths,^[5,6] low exciton binding energies, and bandgap tunability,^[7,8] which are particularly beneficial for photovoltaic (PV) applications. However, the power conversion efficiency (PCE) of a single-junction device is fundamentally limited by the principle of detailed balance.^[9] One way to surpass this limit is to use a tandem cell architecture,^[10–12] where the top cell with a wider bandgap absorbs high-energy photons to produce a higher open-circuit voltage (V_{OC}) and the bottom cell with a narrower bandgap absorbs the remaining low-energy photons. This tandem architecture minimizes the energy losses arising from charge-carrier thermalization and cooling while exhibiting a broad absorption bandwidth compared to a wide-

bandgap single-junction device. Since carefully optimized bandgaps are required for such multi-junction tandem cells to work efficiently, the facile bandgap tunability of MHPs is highly advantageous for tandem cell applications. Bandgap tuning in these materials can be achieved by altering their chemical compositions – MHPs have a chemical formula of ABX_3 , where the A cation site is usually occupied by a methylammonium (MA^+), formamidinium (FA^+) or cesium (Cs^+) ion, the B site by a divalent metal cation such as lead (Pb^{2+}) or tin (Sn^{2+}), and the X halide site by iodide (I^-) or bromide (Br^-), or a mixture thereof. An optimal high bandgap for the top subcell has previously been achieved for silicon-perovskite and all-perovskite tandem cells through tuning of the X halide site occupation in the absorber layer, resulting in a mixed-halide lead perovskite.^[13,14] Compared to a silicon-perovskite tandem cell, an all-perovskite tandem cell offers lower processing temperatures and greater compositional tunability which would be highly desirable in the manufacturing process of the devices.^[12] Because of the strong bandgap bowing effect observed across the Pb-Sn series, mixed lead-tin perovskites offer the lowest possible bandgap achievable in MHPs,^[8,15,16] making them the most promising candidates for

V. J.-Y. Lim, A. M. Ulatowski, M. B. Johnston, L. M. Herz
Department of Physics
Clarendon Laboratory
University of Oxford
Parks Road, Oxford OX1 3PU, UK
E-mail: laura.herz@physics.ox.ac.uk

C. Kamaraki, M. T. Klug, L. Miranda Perez
Oxford PV
Unit 7/8 Mead Road, Yarnton OX5 1QU, UK

C. Kamaraki
Department of Physics
University of Bath
Claverton Down, Bath BA2 7AY, UK

L. M. Herz
Institute for Advanced Study
Technical University of Munich
Lichtenbergstrasse 2a, D-85748 Garching, Germany

 The ORCID identification number(s) for the author(s) of this article can be found under <https://doi.org/10.1002/aenm.202200847>.

© 2022 The Authors. Advanced Energy Materials published by Wiley-VCH GmbH. This is an open access article under the terms of the Creative Commons Attribution License, which permits use, distribution and reproduction in any medium, provided the original work is properly cited.

DOI: 10.1002/aenm.202200847

the bottom subcell of an all-perovskite tandem cell.^[12] Extensive research has also revealed excellent optoelectronic properties of such $\text{APb}_x\text{Sn}_{1-x}\text{I}_3$ MHPs in the region of tin content $x \approx 0.4\text{--}0.6$, for which these perovskites exhibit high charge-carrier mobilities and lifetimes, making them ideal for PV applications.^[15]

Despite their importance to the development of all-perovskite tandem cells, mixed lead-tin halide perovskites still suffer from instabilities when exposed to oxygen and moisture even under encapsulation,^[17] which deteriorate their optoelectronic properties and hinder their commercialization.^[1,17–19] However, a comprehensive evaluation of the degradation pathways in lead-tin halide perovskites is still part of ongoing research. The degradation mechanisms of tin-only halide perovskites have been previously investigated,^[18,20–24] providing potential insight into the degradation pathways of their mixed lead-tin counterparts. Tin-only MHPs suffer from severe oxygen and moisture stability issues, which derive from the formation of tin vacancies and iodide interstitials.^[25,26] The presence of these point defects induces the oxidation of Sn^{2+} to Sn^{4+} ^[27,28] and introduces unintentional p-type doping, leading to the presence of a large density of background holes.^[15] Such oxidation of the metal in the perovskite structure is intensified by the relatively small standard reduction potential of $\text{Sn}^{4+}/\text{Sn}^{2+}$ when compared to $\text{Pb}^{4+}/\text{Pb}^{2+}$ (+0.15 and +1.67 V, respectively).^[25,29] SnF_2 additive has been commonly and successfully used to suppress tin vacancy formation in tin-only perovskites by creating a tin-rich environment during the fabrication process.^[15,23,30,31] There have been suggestions that mixed lead-tin MHPs may undergo similar degradation pathways, involving tin vacancy formation and oxidation. An increase in lead content is expected to result in a gradual transition toward the defect chemistry present in lead-only perovskite, which is mostly free of trap states located deeply in the bandgap.^[26] However, full knowledge of the defect chemistry in mixed lead-tin MHPs is still lacking, with a particular need to contrast the degradation mechanisms of tin-only with those of mixed tin-lead iodide perovskites.

In this study, we have unraveled the differences in the degradation pathways of tin-only and mixed lead-tin MHPs under ambient air. We examined spin-coated $\text{FA}_{0.75}\text{Cs}_{0.25}\text{Pb}_{0.5}\text{Sn}_{0.5}\text{I}_3$ (mixed lead-tin) and $\text{FA}_{0.75}\text{Cs}_{0.25}\text{SnI}_3$ (tin-only) thin perovskite films (fabrication details provided in Section S1, Supporting Information) which have direct relevance to all-perovskite tandem and lead-free single-junction photovoltaics devices, respectively. Both of these compositions were fabricated with the addition of 10 mol% SnF_2 , which has been a frequently adopted additive in previous studies reporting high-performing photovoltaic devices.^[32–35] We investigated the optoelectronic properties of the perovskites in ambient air utilizing a combination of non-contact transient THz photoconductivity measurements and visible absorption spectroscopy, and their structural and vibrational properties employing X-ray diffraction (XRD) as well as infrared and THz transmission spectroscopy. We found that degradation in tin-only $\text{FA}_{0.75}\text{Cs}_{0.25}\text{SnI}_3$ can be explained almost exclusively by tin-vacancy formation and self-doping effects. However, we demonstrate that for intermediate mixed lead-tin MHPs this is not the prevalent degradation pathway. We instead propose that degradation of lead-tin iodide perovskites in ambient air involves the formation of deep trap states, which do not contribute to

the significant doping of the MHP. Our findings thus highlight that stability improvements for mixed lead-tin perovskites likely require different defect passivation methods to those already developed for their tin-only counterparts.

2. Results and Discussion

We commence our study by investigating the effect of ambient air exposure on the optoelectronic properties of $\text{FA}_{0.75}\text{Cs}_{0.25}\text{Pb}_x\text{Sn}_{1-x}\text{I}_3$ thin films, contrasting the mixed lead-tin material $\text{FA}_{0.75}\text{Cs}_{0.25}\text{Pb}_{0.5}\text{Sn}_{0.5}\text{I}_3$ with its tin-only $\text{FA}_{0.75}\text{Cs}_{0.25}\text{SnI}_3$ equivalent (full fabrication protocols are provided in Section 1, Supporting Information). Assessing such changes in the optoelectronic quality of the materials under air degradation is critical for photovoltaic applications which rely on photo-generated charge carriers being able to travel across the full thickness of the active layer to the respective transport layers and electrodes for the efficient generation of electrical power. High charge-carrier diffusion lengths are essential to this process and depend on high electronic mobilities and low charge-carrier recombination rates.^[36] Therefore, to assess the effect of oxygen and moisture exposure on the optoelectronic properties of the materials, we measured the changes occurring in their photoinduced conductivity dynamics during exposure to ambient air of $45 \pm 10\%$ humidity over hundreds of minutes. We employed the optical-pump terahertz-probe (OPTP) spectroscopic technique,^[37] for which the films are excited with an ultrafast pump laser pulse, and their time-dependent photo-induced conductivity is measured by THz probe-pulse transmission, as detailed in Section 2 (Supporting Information).

Figure 1a shows examples of photoconductivity decay transients measured for a $\text{FA}_{0.75}\text{Cs}_{0.25}\text{SnI}_3$ thin film at different air-exposure times (full data sets for both $\text{FA}_{0.75}\text{Cs}_{0.25}\text{SnI}_3$ and $\text{FA}_{0.75}\text{Cs}_{0.25}\text{Pb}_{0.5}\text{Sn}_{0.5}\text{I}_3$ are provided in Section S2.1, Supporting Information). With increasing air exposure, the photoconductivity amplitude following initial photoexcitation declines. This trend can be understood given that the conductivity σ of the material depends on the charge-carrier pair density n and the electron-hole sum mobility μ according to $\sigma = en\mu$, where e is the elementary charge. The mobility of the charge carriers can therefore be extracted from the THz transmission immediately after photoexcitation (time = 0) before any charge-carrier recombination events may have occurred (full description of data analysis provided in Section S2.1, Supporting Information). The subsequent decay of the photoconductivity over time after excitation is associated with the decline of charge-carrier population $n(t)$, therefore providing insight into the charge-carrier recombination dynamics. We find that the photoconductivity transients can be well described by a monoexponential decay function, $n(t) = n_0 \exp(-k_1t)$, with fits displayed as solid lines on top of measured data shown in hollow hoops. The majority of charge carriers thus recombine through monomolecular channels, which could arise, e.g., from trap-mediated recombination or electron recombination with a significantly larger density of background holes, both of which depend on the dynamics of only one charge-carrier species.^[31] From these monoexponential fits (full data set and fits shown in

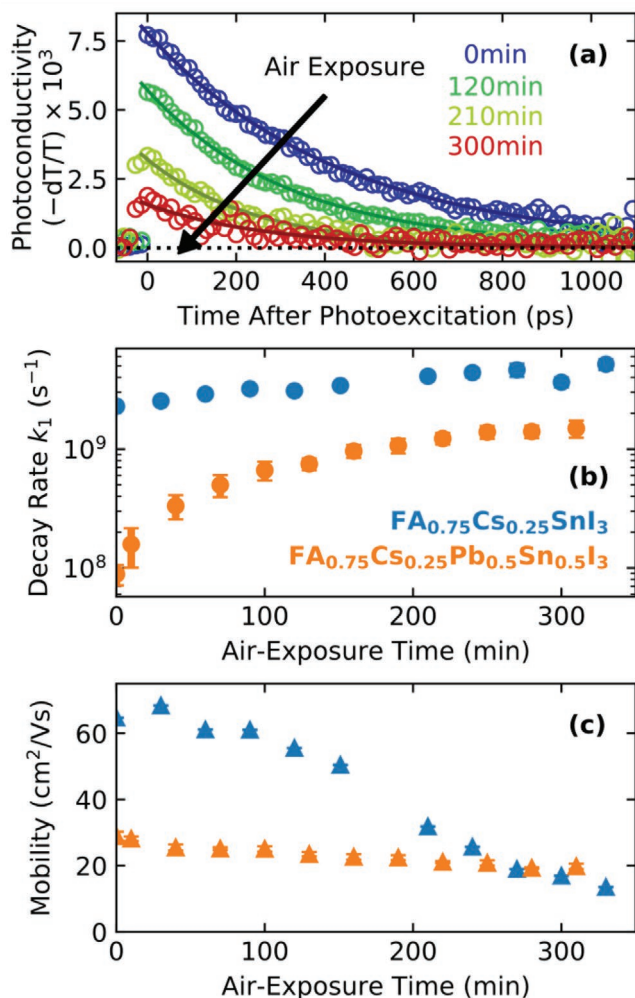


Figure 1. a) Photoconductivity decay transients obtained from optical-pump THz-probe photoconductivity measurements performed on $FA_{0.75}Cs_{0.25}SnI_3$ with 400 nm photoexcitation and fluence of $3.6 \mu J cm^{-2}$ at discrete air-exposure (degradation) times in ambient air (full data set available in Section S2.1, Supporting Information). b) Monomolecular charge-carrier recombination rates (k_1 , shown in solid circles) and c) charge-carrier mobilities (solid triangles) of $FA_{0.75}Cs_{0.25}SnI_3$ (blue) and $FA_{0.75}Cs_{0.25}Pb_{0.5}Sn_{0.5}I_3$ (orange) thin films were extracted from THz photoconductivity measurements shown in (a) and Figures S2 and S3 (Supporting Information), as detailed in Section S2.1 (Supporting Information).

Figure S2 and S3 (Supporting Information)) we extracted values for the decay rate k_1 (shown in Figure 1b) and electron-hole sum mobility μ (Figure 1c) for both $FA_{0.75}Cs_{0.25}SnI_3$ and $FA_{0.75}Cs_{0.25}Pb_{0.5}Sn_{0.5}I_3$ thin films and plotted them against degradation time in air. These data reveal a clear rise in recombination rates and a decrease in charge-carrier mobility for both materials with air exposure. As shown in Figure S4 (Supporting Information), the combined effect has disastrous consequences for the charge-carrier diffusion length L_D in the two materials: for $FA_{0.75}Cs_{0.25}SnI_3$, air exposure over 5 h leads to a three-fold decline of L_D from 270 to 80 nm while for $FA_{0.75}Cs_{0.25}Pb_{0.5}Sn_{0.5}I_3$, L_D falls from initially 910 to 220 nm.

Surprisingly, Figure 1b reveals that the relative increase in the recombination rate with extended air exposure is far smaller for $FA_{0.75}Cs_{0.25}SnI_3$ than for its lead-tin equivalent, even though the initial rate for the pristine thin film is significantly higher. This observation indicates^[31] that as-fabricated $FA_{0.75}Cs_{0.25}SnI_3$ is more prone to defect formation even in the absence of sizeable exposure to oxygen or moisture. This difference arises from marked changes in the defect chemistry along the lead-tin solid solution line, as predicted previously from theoretical calculations,^[26] which will be discussed in more detail later below. Conversely, the low initial value of the decay rate k_1 for $FA_{0.75}Cs_{0.25}Pb_{0.5}Sn_{0.5}I_3$ suggests inherently better resistance during fabrication to the type of defects accelerating monomolecular recombination, however, the significant increase in the recombination rate after air exposure highlights the clear need for highly air-impermeable encapsulation of PV devices employing these absorbers.

Interestingly, Figure 1c shows that the air-induced acceleration of defect-related charge-carrier recombination affects the charge-carrier mobilities of $FA_{0.75}Cs_{0.25}SnI_3$ and $FA_{0.75}Cs_{0.25}Pb_{0.5}Sn_{0.5}I_3$ to different extents. In general, defect formation is expected to be accompanied by a decrease in charge-carrier mobility because of the introduction of scattering centers. However, while $FA_{0.75}Cs_{0.25}Pb_{0.5}Sn_{0.5}I_3$ exhibits the strongest increase in recombination rate (Figure 1b), its decline of mobilities (Figure 1c) with air exposure is much more gradual than that observed for $FA_{0.75}Cs_{0.25}SnI_3$. The tin-only $FA_{0.75}Cs_{0.25}SnI_3$ initially exhibits higher mobility prior to air exposure, which intrinsically results from fundamentally lower effective masses of charge carriers, and higher energies of the optical phonon mode in tin halide perovskites compared to lead-halide perovskites.^[31,38] However, the charge-carrier mobility for $FA_{0.75}Cs_{0.25}SnI_3$ decreases drastically to only $\approx 20\%$ of its initial value over the first ≈ 300 min of air exposure, while for $FA_{0.75}Cs_{0.25}Pb_{0.5}Sn_{0.5}I_3$, this decline is much less severe, to $\approx 80\%$ its initial value after the same degradation time. This finding suggests that although both materials experience significant defect formation during air-induced degradation, the types of defects forming in tin-only MHPs are more detrimental to the charge-carrier mobility than those formed in mixed Pb-Sn perovskites.

These observations provide clues to the differences in the defect chemistry of tin-rich and intermediate lead-tin halide perovskites. Tin-rich perovskites are prone to tin vacancy formation, which may be accompanied by tin oxidation and iodine interstitial formation.^[26] Tin vacancies are known to cause background p-doping of the MHP material by introducing defect states within the valence band that capture electrons and therefore effectively release free holes into the semiconductor.^[26] Such p-doping deteriorates optoelectronic properties of the material by increasing the charge-carrier recombination rates through the introduction of additional recombination pathways, for example through radiative recombination of photogenerated electrons with background holes that are present in high density.^[39] Concurrently, such effects will reduce charge-carrier mobility because tin vacancies will be negatively charged following free hole release, making them particularly effective scattering centers to mobile charge carriers.^[30,31] In addition, charge-carrier scattering with rates in the femtosecond regime^[30] may reduce their mobilities in the

presence of substantial hole densities resulting from such self-doping. In contrast, intermediate lead-tin iodide perovskites appear to exhibit a different type of degradation pathway for which the defects formed do not possess significant scattering cross-section, as evidenced by relatively unchanged charge-carrier mobility over the measurement time window accompanying the sharp increase in recombination rates. The significant increase in photoconductivity decay rate k_1 for $\text{FA}_{0.75}\text{Cs}_{0.25}\text{Pb}_{0.5}\text{Sn}_{0.5}\text{I}_3$ under air exposure is therefore most likely associated with the formation of defects that are charge-neutral, which would result in lower scattering cross-section and would not lead to electrical doping.

To explore such differences in air-degradation mechanisms of $\text{FA}_{0.75}\text{Cs}_{0.25}\text{SnI}_3$ and $\text{FA}_{0.75}\text{Cs}_{0.25}\text{Pb}_{0.5}\text{Sn}_{0.5}\text{I}_3$ films further, we assessed the effect of air-exposure on their electronic structure. The absorption spectrum of a thin film provides an insight into the electronic structure of the material, enabling evaluation of the bandgap and exciton binding energies. In general, the absorption spectrum of a semiconductor displays a continuum band-to-band absorption above its bandgap energy E_g , which is enhanced by electron-hole Coulomb interactions, and a resonant absorption peak below E_g , owing to the formation of a bound electron-hole excitonic state. Changes to the bandgap of material would then lead to a shift of the whole spectrum in energy, whereas changes to the strength of exciton binding energies E_b would mostly moderate the absorption onset at low energies. Figure 2a and c show changes in the absorption spectrum over ≈ 15 h of air exposure for $\text{FA}_{0.75}\text{Cs}_{0.25}\text{SnI}_3$ and $\text{FA}_{0.75}\text{Cs}_{0.25}\text{Pb}_{0.5}\text{Sn}_{0.5}\text{I}_3$ films, respectively. The significant change observed for the low-energy part of the absorption spectrum of tin-only $\text{FA}_{0.75}\text{Cs}_{0.25}\text{SnI}_3$ could in principle be caused by either the Burstein-Moss effect or a decrease in the exciton binding energy. Burstein-Moss effects^[31,40,41] are prominent in tin-rich perovskites^[30,31,42] owing to the presence of high hole densities resulting from tin vacancies and the resulting unintentional doping, which lowers the Fermi level and partially depletes the valence band

of electrons. As a result, light absorption is only possible from states deeper into the valence band, blue-shifting the absorption edge of the material without significantly affecting the continuum absorption at higher energies.^[31,40,41] In addition, such an increase in the background hole density may also affect the exciton binding energy through enhanced electronic screening of the Coulomb attraction that binds excitons.^[15,43] To unravel these effects, we performed fits according to Elliott theory^[44] which describes the absorption of a semiconductor in the presence of Coulomb interactions (as detailed in Section S3.1, Supporting Information), with the resulting values for the bandgap E_g and exciton binding energy E_b displayed as a function of air-exposure time in Figure 2b and d for $\text{FA}_{0.75}\text{Cs}_{0.25}\text{SnI}_3$ and $\text{FA}_{0.75}\text{Cs}_{0.25}\text{Pb}_{0.5}\text{Sn}_{0.5}\text{I}_3$, respectively.

Our analysis demonstrates that for $\text{FA}_{0.75}\text{Cs}_{0.25}\text{SnI}_3$, both Burstein-Moss effect and exciton screening gain significant prominence as the tin-only material is exposed to air, as revealed by an increase in the effective bandgap and a decrease of the binding energy. As explained above, these observations are consistent with a significant amount of electronic doping being introduced into the material during the degradation process, most likely arising from the tin-vacancy formation. For the mixed lead-tin $\text{FA}_{0.75}\text{Cs}_{0.25}\text{Pb}_{0.5}\text{Sn}_{0.5}\text{I}_3$ perovskite, on the other hand, the evolution of the absorption spectrum and the corresponding Elliott fitting (Figure 2c,d) imply only very minor changes in the effective bandgap and exciton binding energies, even over long (≈ 15 h) air-exposure times. Thus, we conclude that, in contrast to tin-only $\text{FA}_{0.75}\text{Cs}_{0.25}\text{SnI}_3$, the defects in mixed lead-tin $\text{FA}_{0.75}\text{Cs}_{0.25}\text{Pb}_{0.5}\text{Sn}_{0.5}\text{I}_3$ causing the observed optoelectronic degradation under air do not introduce free charge carriers into the conduction or valence bands. We therefore propose that accelerated charge-carrier recombination arising from air exposure of $\text{FA}_{0.75}\text{Cs}_{0.25}\text{Pb}_{0.5}\text{Sn}_{0.5}\text{I}_3$ is instead mediated by the introduction of a large density of deep trap states, whose energy level lies significantly further from the band edge than thermal energy at room temperature, and which do not electrically dope the material to a significant extent.^[45]

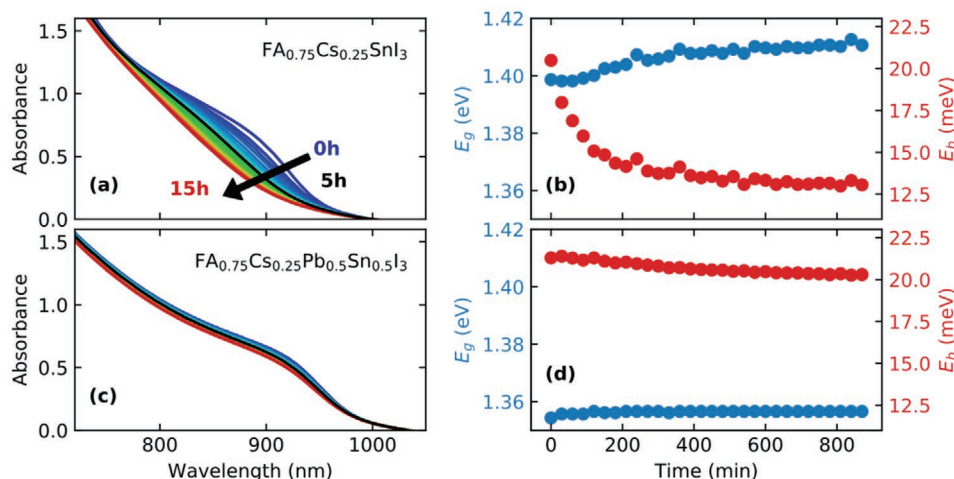


Figure 2. Absorbance spectra of an a) $\text{FA}_{0.75}\text{Cs}_{0.25}\text{SnI}_3$ and c) $\text{FA}_{0.75}\text{Cs}_{0.25}\text{Pb}_{0.5}\text{Sn}_{0.5}\text{I}_3$ thin-film recorded at 30 min intervals over ≈ 15 h of ambient-air exposure. The absorbance spectra at 5 h of exposure are highlighted in black solid lines for comparison with the time scales for OPTP data shown in Figure 1. The corresponding bandgap energy (E_g) and exciton binding energy (E_b) extracted for (c) $\text{FA}_{0.75}\text{Cs}_{0.25}\text{SnI}_3$ and d) $\text{FA}_{0.75}\text{Cs}_{0.25}\text{Pb}_{0.5}\text{Sn}_{0.5}\text{I}_3$ from Elliott fitting as detailed in Section S3.1 (Supporting Information).

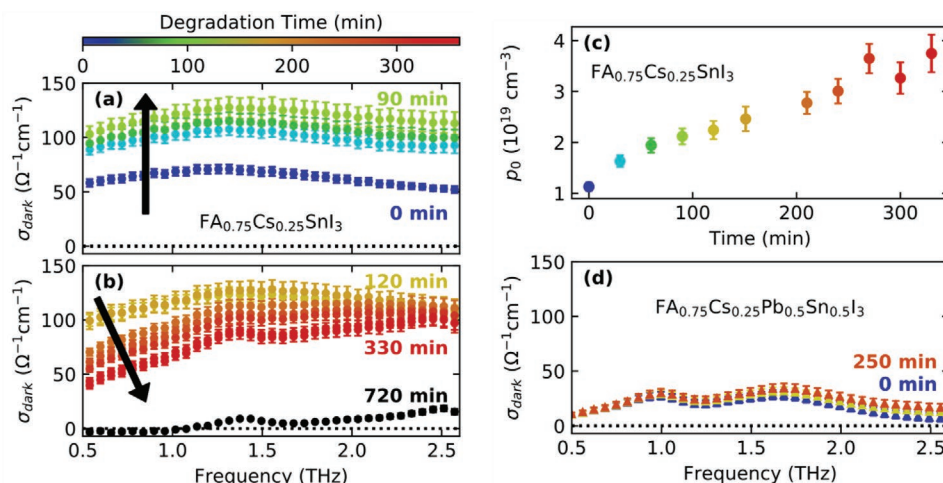


Figure 3. a,b) Dark conductivity spectra of a $\text{FA}_{0.75}\text{Cs}_{0.25}\text{SnI}_3$ thin film measured at different degradation times in ambient air as indicated by the color-coded legend. c) Estimated background hole density extracted from spectra in (a) and (b), as detailed in Section S4.2 (Supporting Information), plotted against exposure time in ambient air. d) Dark conductivity spectra of a $\text{FA}_{0.75}\text{Cs}_{0.25}\text{Pb}_{0.5}\text{Sn}_{0.5}\text{I}_3$ thin film at different degradation times in ambient air.

We further confirm the strongly enhanced presence of electrical doping in tin-only $\text{FA}_{0.75}\text{Cs}_{0.25}\text{SnI}_3$ in air, and the lack of major doping in its mixed lead-tin $\text{FA}_{0.75}\text{Cs}_{0.25}\text{Pb}_{0.5}\text{Sn}_{0.5}\text{I}_3$ counterpart, by performing measurements of THz conductivity spectra in the absence of photoexcitation during their degradation in ambient air. Dark conductivity spectra shown in **Figure 3a,b** confirm the monotonic increase of background doping density for $\text{FA}_{0.75}\text{Cs}_{0.25}\text{SnI}_3$ with air-exposure time, in contrast to $\text{FA}_{0.75}\text{Cs}_{0.25}\text{Pb}_{0.5}\text{Sn}_{0.5}\text{I}_3$ (**Figure 3d**) which did not exhibit signs of electric background doping or changes in dark conductivity with air exposure within our detection limit. We note that such dark THz conductivity spectra are equivalent to measurements of the dielectric function at THz frequencies. As such, these may provide information about not only the presence of a background charge-carrier density arising, e.g., from unintentional doping, but also on vibrational absorptions falling into the THz frequency region. In our analysis below, we disentangle such effects (additional details are provided in Section S4.2, Supporting Information). Measurements of the dark conductivity spectra were performed with terahertz time-domain spectroscopy (THz-TDS) at different air-exposure times, as detailed in Section S4.1, (Supporting Information).

For tin iodide perovskites, a recent analysis of dark THz conductivity spectra has shown these to be dominated by relatively broad phonon modes and a strong free-charge response arising from a substantial hole background density.^[31] Such Drude-like conductivity of charge carriers in metal halide perovskites is known to be spectrally flat across the THz frequency range, owing to the relatively fast momentum scattering.^[30,31] We therefore expect the dark conductivity response of tin iodide perovskites to shift vertically toward higher conductivities as the density of background charge carriers increases with air-exposure time, which is exactly what we observe for $\text{FA}_{0.75}\text{Cs}_{0.25}\text{SnI}_3$ for early degradation times (**Figure 3a**) over the first ≈ 90 min of air exposure. We note however that at later times beyond ≈ 120 min in air, the background conductivity decreases again in amplitude (**Figure 3b**) which we attribute to the decrease of the charge-carrier mobility observed in **Figure 1c** that accompanies

a continued increase in background hole density arising from the tin-vacancy formation. To disentangle such effects, we separate the two contributions of the hole mobility μ_h and the background hole density p_0 to the dark conductivity, given by $\sigma = ep_0\mu_h$, considering the values of mobility extracted from OPTP measurements (**Figure 1c**) at various degradation times and selecting a spectral range for analysis where phonons make little contribution (as detailed in Section S4.2, Supporting Information). We present the background hole density extracted in this manner for $\text{FA}_{0.75}\text{Cs}_{0.25}\text{SnI}_3$ in **Figure 3c**, and find that it exhibits a monotonic increase with degradation time in air, rising from 1×10^{19} to $4 \times 10^{19} \text{ cm}^{-3}$ after ≈ 5 h in air. This increase in unintentional doping further corroborates the formation of shallow defect acceptor states, such as tin vacancies, as the main air-degradation mechanism in tin-only $\text{FA}_{0.75}\text{Cs}_{0.25}\text{SnI}_3$.

Such background doping is in contrast to what is observed for the mixed lead-tin $\text{FA}_{0.75}\text{Cs}_{0.25}\text{Pb}_{0.5}\text{Sn}_{0.5}\text{I}_3$ film (**Figure 3d**), whose dark conductivity spectrum remains mostly unchanged with degradation time and simply displays two vibrational peaks associated with optical phonon modes of the metal-iodide sublattice.^[30,31] The lack of change of these spectra with time and the absence of a spectrally flat Drude-like (free-charge) conductivity signature implies that for $\text{FA}_{0.75}\text{Cs}_{0.25}\text{Pb}_{0.5}\text{Sn}_{0.5}\text{I}_3$, any unintentional doping arising from tin vacancies is comparatively low ($< 10^{18} \text{ cm}^{-3}$, according to our detection limit, see Section S4.2, Supporting Information), despite the high (50%) content of tin in the structure and the optoelectronic degradation observed in **Figure 1**. This result is consistent with our earlier finding that exciton screening and Burstein-Moss effects are not observed in the absorption spectra of this material. We, therefore, conclude that the air degradation of $\text{FA}_{0.75}\text{Cs}_{0.25}\text{Pb}_{0.5}\text{Sn}_{0.5}\text{I}_3$ predominantly involves the formation of defect states deep within the bandgap, i.e., defects whose energy levels do not lie close to or within the bands. These deep traps effectively induce trap-mediated recombination, increasing the monomolecular recombination rates, but do not curtail the charge-carrier mobilities as severely as the charged tin vacancies prevalent in tin-only iodide perovskites.

Furthermore, the THz dark conductivity spectrum of tin-only $\text{FA}_{0.75}\text{Cs}_{0.25}\text{SnI}_3$ also allows us to garner additional information on its degradation products under prolonged air exposure. After 12 h in air (black dots in Figure 3b) the spectra reveal two new peaks appearing after degradation, which occur at higher frequencies (at 1.4 and 2.5 THz) than those associated with the optical modes of the metal-iodide perovskite sub-lattice^[31] and therefore must be of a different origin. We note that the clear visibility of these peaks suggests that charge-carrier mobilities have now been so significantly impacted by degradation that any background hole densities present can no longer effectively contribute to the overall photoconductivity. We deduce that these new phonon modes arise from vacancy-ordered double perovskite formation in the material resulting from tin oxidation in the presence of air. Previously reported degradation products from the decomposition of ASnI_3 perovskites in ambient air include SnI_4 , SnO_2 as well as a double-perovskite A_2SnI_6 ,^[18,20,46,47] arising from the better stability of the 4+ oxidation state over the 2+ state in tin. Since every other metal site of the vacancy-ordered perovskite is empty, the equivalent reduced ionic mass of the crystalline structure is lower than for a standard ABX_3 perovskite. From a simplified picture of vibrations in a diatomic chain, this lowering of ionic reduced mass is expected to increase the frequency of oscillation (phonon) modes compared to those seen in the equivalent ABX_3 perovskite structure. The two peaks at 1.4 and 2.5 THz are therefore attributed to the optical phonon modes of the equivalent vacancy-order double perovskite, and we note that those frequencies indeed agree with the transverse-optical phonon modes of vacancy-ordered Cs_2SnI_6 previously reported,^[48] as fully discussed in Section S6 (Supporting Information). Therefore, prolonged air exposure of $\text{FA}_{0.75}\text{Cs}_{0.25}\text{SnI}_3$ ultimately leads to tin oxidation and chemical decomposition toward vacancy-ordered double perovskites, following on from the initial tin vacancy formation.

Finally, we investigate the structural properties of the $\text{FA}_{0.75}\text{Cs}_{0.25}\text{SnI}_3$ and $\text{FA}_{0.75}\text{Cs}_{0.25}\text{Pb}_{0.5}\text{Sn}_{0.5}\text{I}_3$ films through X-ray diffraction (XRD) measurements, in order to assess changes occurring during their degradation in ambient air over a prolonged time of air exposure. The evolution of the second-order quasi-cubic (200) X-ray diffraction peaks is presented in Figure 4 over an air-exposure time window of 72 h (full XRD spectra over a wider 2θ range in Section S5, Supporting Information). We find that both materials exhibit only relatively minor structural changes over the first few hours of air exposure, during which the optoelectronic properties of the film have been found to deteriorate significantly, as highlighted by the OPTP and THz-TDS measurements discussed above (Figure 1). This observation further confirms that the optoelectronic degradation we reported on for air exposure over the first ≈ 5 h was a result of point-defect formation, rather than full structural deterioration of the semiconductors. We note that for longer air exposure, however, the XRD peak amplitude decreases substantially, suggesting a loss of the perovskite structure and a potential formation of degradation products.

For tin-only $\text{FA}_{0.75}\text{Cs}_{0.25}\text{SnI}_3$, an extended air exposure (≈ 72 h) results in the (200) perovskite peak no longer being observable, but a broad, weak peak instead arises at a higher diffraction angle 2θ (Figure 4a inset). XRD peaks of vacancy-ordered

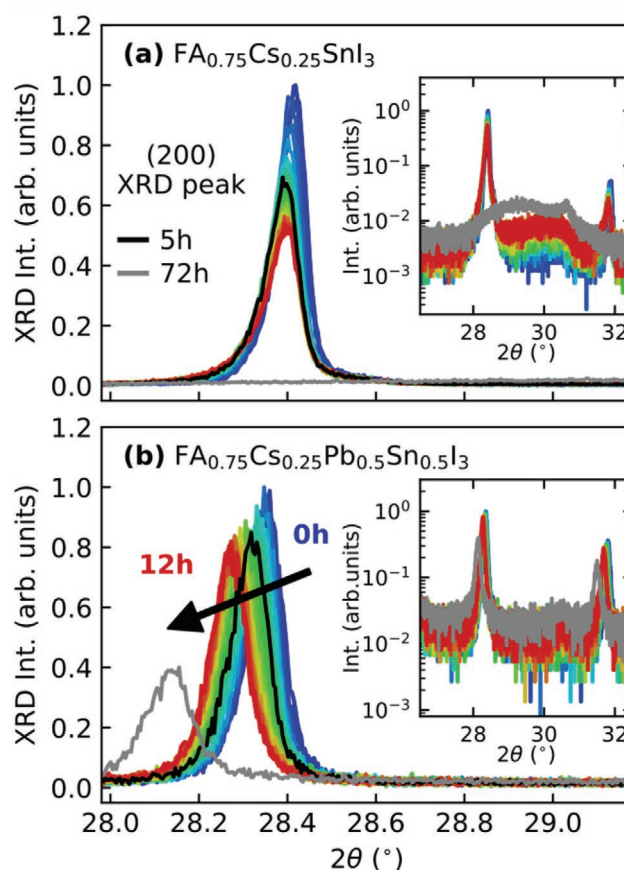


Figure 4. (200) X-ray diffraction peaks of a) $\text{FA}_{0.75}\text{Cs}_{0.25}\text{SnI}_3$ and b) $\text{FA}_{0.75}\text{Cs}_{0.25}\text{Pb}_{0.5}\text{Sn}_{0.5}\text{I}_3$ thin films measured at 30 min intervals over the first ≈ 12 h of ambient-air degradation and again at 72 h. Insets show the results of the same measurement over a broader angle range and plotted on a logarithmic scale. The spectra at 5 h exposure time are highlighted with a black solid line for comparison with OPTP and THz-TDS data, and the spectra at 72 h are denoted with grey lines.

double perovskites are expected to appear at a higher diffraction angle than those of their equivalent perovskite counterpart, since the enhanced oxidation state of tin ions decreases the lattice parameter, in agreement with previous reports.^[20,46,47,49] Therefore, we attribute the broad peak observed for tin-only $\text{FA}_{0.75}\text{Cs}_{0.25}\text{SnI}_3$ to the formation of a vacancy-ordered double perovskite, in agreement with our analysis of dark conductivity spectra above. The broad nature of the peak indicates that the size of such double perovskite domains must be small, leading to X-ray diffraction off relatively few lattice planes for each such inclusion. Prolonged air-induced degradation of $\text{FA}_{0.75}\text{Cs}_{0.25}\text{SnI}_3$ therefore ultimately leads to a highly structurally, and most likely also compositionally, disordered material.

The mixed lead-tin $\text{FA}_{0.75}\text{Cs}_{0.25}\text{Pb}_{0.5}\text{Sn}_{0.5}\text{I}_3$ film, on the other hand, shows a much slower decrease in XRD peak amplitude (Figure 4b) and an absence of any discernable vacancy-ordered double perovskite, even after 72 h of ambient air exposure. The relatively slow deterioration in its structure (Figure 4) in the presence of a much more rapid decline in its optoelectronic properties (Figure 1) again suggests that the former is caused by the introduction of point defects that leave the perovskite

structure fundamentally intact. However, a small increase in the lattice parameter of the crystal structure with degradation is evidenced by the XRD peak shifting to a lower 2θ angle with prolonged air exposure. We attribute this shift to an effect related to the A-cation composition ($\text{FA}_{0.75}\text{Cs}_{0.25}$), given that the same measurements were conducted on a $\text{FA}_{0.6}\text{MA}_{0.4}\text{Pb}_{0.5}\text{Sn}_{0.5}\text{I}_3$ film (presented in Figure S8 and S9, Supporting Information) but reveal a lack of such lattice contraction. We note that such differences in the decomposition pathways associated with A-cation site composition in mixed lead-tin MHPs are beyond the scope of this study but will be investigated in future work.

To summarize, we have shown that tin-only $\text{FA}_{0.75}\text{Cs}_{0.25}\text{SnI}_3$ perovskite degrades in air via heavy p-type self-doping of the semiconductor, originating from the formation of a high density of shallow tin-vacancy point defects, in agreement with previous reports.^[15,27,30,31] SnF_2 addition has been widely and successfully used as an additive to suppress such tin-vacancy formation during the deposition process.^[31,42] However, our work here revealed that air degradation of mixed lead-tin $\text{FA}_{0.75}\text{Cs}_{0.25}\text{Pb}_{0.5}\text{Sn}_{0.5}\text{I}_3$ instead results in the formation of much deeper trap states, with electrical doping being far less prominent in the material than in the tin-only equivalent. There have been suggestions based on theoretical calculations^[26] that mixed lead-tin perovskites (specifically $\text{MAPb}_{0.5}\text{Sn}_{0.5}\text{I}_3$) might potentially be free of trap states energetically situated near mid-bandgap. However, energy levels calculated for tin vacancies, iodide vacancies and tin interstitials in such mixed lead-tin perovskites all lie within the bandgap, and, importantly, are situated more than the thermal energy at room temperature ($k_{\text{B}}T \approx 25$ meV) away from the band edges,^[26] therefore these are potential candidates for the trap-mediated recombination pathways observed herein. We note that the formation of tin and iodide vacancies is also consistent with a recent surface probe of the degradation of lead-tin perovskites employing X-ray photoelectron spectroscopy.^[50] We note that while tin vacancies are dominant shallow defect states in tin-only perovskites, the lowering of the valence band upon substitution of lead (owing to enhanced spin-orbit coupling) may turn such vacancies into deep trap states in mixed tin-lead perovskites,^[26] thus trap-mediated recombination in the absence of significant self-doping may occur, as we observe. However, it has been postulated that tin-vacancy formation is suppressed once a significant fraction of tin has been replaced with lead in these perovskites.^[15,18,26,38] Given that $\text{FA}_{0.75}\text{Cs}_{0.25}\text{Pb}_{0.5}\text{Sn}_{0.5}\text{I}_3$ shows substantially more rapid increase in charge-carrier recombination rates with air exposure than $\text{FA}_{0.75}\text{Cs}_{0.25}\text{SnI}_3$ (Figure 1b), it is therefore perhaps more likely that such deep-trap formation in intermediate tin-lead compositions is caused by iodide vacancies, which form prominent deep-level defects in lead iodide perovskites.^[26,51–53] Overall, we highlight the differences we observe in the electronic behavior of these perovskites, contrasting shallow, hole-donating defect states formed in tin-only perovskites, with deep-trap states formed in mixed lead-tin perovskites, which do not significantly contribute to background doping, but lead to optoelectronic deterioration. We, therefore, suggest further investigation into novel fabrication methods of mixed lead-tin perovskites, including the exploration of an iodide-rich environment to prevent iodide vacancies, and further optimization of the tin-additive concentration in order to carefully balance the

trade-off between tin-vacancy and tin-interstitial formation. We also note that a stronger focus is needed on eliminating tin inhomogeneities^[54] as these may result in lead-tin perovskites with nominally optimized tin stoichiometry, but exhibiting a combination of locally tin-rich environments where tin interstitials are dominant, and locally tin-poor environment where tin vacancies are dominant. Since either defect type represents an electronic trap, a simple addition of SnF_2 may be insufficient if this treatment fails to induce fully homogeneous tin addition on the metal sites. An alternative possibility is the formation of SnO_2 within the mixed lead-tin perovskite structure during air-degradation, which has been suggested in previous reports and could also result in a deterioration of optoelectronic properties of the semiconductor.^[15,18,20,25,50] Owing to the abundance of the defect states present within SnO_2 inclusions and at their interface with perovskite crystals,^[55–61] even a relatively low density of SnO_2 may decrease the charge-carrier recombination rate, without much affecting the charge-carrier mobility measured with terahertz spectroscopy. The amorphous and disordered nature of these SnO_2 domains means that they can rarely be observed in XRD patterns, providing a plausible explanation for our findings of declined optoelectronic properties in tin-lead perovskites in the absence of discernable changes in XRD patterns.^[62] We note that thin-film fabrication in a tin-poor environment may also be able to reduce such SnO_2 formation after air exposure.

3. Conclusion

In conclusion, we have investigated the differences in degradation pathways between $\text{FA}_{0.75}\text{Cs}_{0.25}\text{SnI}_3$ and $\text{FA}_{0.75}\text{Cs}_{0.25}\text{Pb}_{0.5}\text{Sn}_{0.5}\text{I}_3$ perovskite thin films in ambient air. We first identified self p-doping via tin-vacancy formation as the main degradation pathway in the tin-only perovskite, in agreement with previous reports. Such p-doping was evidenced by the Burstein-Moss effect and a decrease of exciton binding energy (E_{b}) of the tin-only perovskite observed during air exposure, as well as an increase in the Drude-like dark conductivity spectrum of the film from the enhancement of the free charge-carrier population. A vacancy-ordered double perovskite structure was also identified as a degradation product, as evidenced by its phonon modes and the appearance of new XRD peaks. The tin-only perovskite also simultaneously underwent deterioration of the optoelectronic properties resulting from charge-carrier recombination of doping-induced holes with photoexcited electrons. These holes, together with negatively charged tin-vacancy complements, act as additional scattering centers, decreasing the momentum scattering time of free charge carriers. Such optoelectronic degradation was observed as a decrease in the charge-carrier mobility (μ) and an increase in charge-carrier recombination rate (k_1), and correspondingly a decrease in the charge-carrier diffusion length (L_{D}). In contrast, air exposure of the mixed lead-tin perovskite predominantly resulted in the formation of deep trap states rather than significant electronic doping. The lack of any discernable change in the dark conductivity spectrum of the lead-tin perovskite, as well as only minor changes to its absorption spectrum during hours of air exposure, suggest that shallow, hole-donating defect states are not the most

abundant defects forming in the mixed tin-lead perovskite upon air exposure. However, despite the lack of significant electronic doping or structural degradation, $\text{FA}_{0.75}\text{Cs}_{0.25}\text{Pb}_{0.5}\text{Sn}_{0.5}\text{I}_3$ exhibited deterioration of its optoelectronic properties upon air exposure, implying the formation of deep-level defect states that accelerate the monomolecular recombination of free carriers. SnF_2 addition has been successful in suppressing the tin-vacancy formation in tin-only perovskite, but our work suggests that this may not necessarily be the right approach for mixed lead-tin perovskites. The $\text{FA}_{0.75}\text{Cs}_{0.25}\text{Pb}_{0.5}\text{Sn}_{0.5}\text{I}_3$ films examined here were produced with a 10% SnF_2 addition, currently the standard for absorber layers incorporated in high-performing perovskite solar cells,^[32,33,34,35] yet they are still liable to deep-trap formation in ambient air. Tin interstitials and iodide vacancies are likely the prominent defect states formed during air degradation of mixed lead-tin perovskites. In addition, given the shifts in predominantly the valence band, any remnant tin vacancies may now form traps deeper in the bandgap, rather than the shallow hole-donating defect states they constitute in tin-only counterparts.^[26] We, therefore, suggest that the suppression of such defect states requires further investigation into iodine-rich fabrication environments, as well as precise balancing of tin content in combination with further exploration of treatments that allow for better tin homogeneity control. Our study highlights the urgent need for the development of additional and alternative passivation methods tuned specifically toward mixed lead-tin perovskites. Such treatments will ultimately improve air stability, enabling all-perovskite tandem devices to become commercially viable with excellent long-term power conversion efficiencies.

Supporting Information

Supporting Information is available from the Wiley Online Library or from the author.

Acknowledgements

The authors acknowledge the Engineering and Physical Sciences Research Council (EPSRC) for financial support. V.J.Y.L. thanks Oxford Photovoltaics and the Prosperity Partnership (EPSRC grant number EP/S004947/1) for financial support. A.M.U. thanks the EPSRC Centre for Doctoral Training in Plastic Electronics for financial support. V.J.Y.L. and A.M.U. thanks the Rank Prize for financial support through a Return to Research grant. C.K. would like to acknowledge funding from the European Union's Horizon 2020 Framework Program for funding Research and Innovation under Grant Agreement No. 764787 (MAESTRO). L.M.H. acknowledges support through a Hans Fischer Senior Fellowship from the Technical University of Munich's Institute for Advanced Study, funded by the German Excellence Initiative.

Conflict of Interest

C.K., M.T.K., and L.M.P. are employees at Oxford PV, a company commercializing perovskite photovoltaics.

Data Availability Statement

The data that support the findings of this study are available from the corresponding author upon reasonable request.

Keywords

degradation, mixed lead-tin perovskites, perovskite solar cells, tandem, trap states

Received: March 11, 2022

Revised: April 16, 2022

Published online:

- [1] S. Sahare, H. D. Pham, D. Angmo, P. Ghoderao, J. MacLeod, S. B. Khan, S. Lee, S. P. Singh, P. Sonar, *Adv. Energy Mater.* **2021**, *11*, 2101085.
- [2] M. Jeong, I. W. Choi, E. M. Go, Y. Cho, M. Kim, B. Lee, S. Jeong, Y. Jo, H. W. Choi, J. Lee, J.-H. Bae, S. K. Kwak, D. S. Kim, C. Yang, *Science* **2020**, *369*, 1615.
- [3] M. B. Johnston, L. M. Herz, *Acc. Chem. Res.* **2016**, *49*, 146.
- [4] S. De Wolf, J. Holovsky, S.-J. Moon, P. Löper, B. Niesen, M. Ledinsky, F.-J. Haug, J.-H. Yum, C. Ballif, *J. Phys. Chem. Lett.* **2014**, *5*, 1035.
- [5] S. D. Stranks, G. E. Eperon, G. Grancini, C. Menelaou, M. J. P. Alcocer, T. Leijtens, L. M. Herz, A. Petrozza, H. J. Snaith, *Science* **2013**, *342*, 341.
- [6] G. Xing, N. Mathews, S. Sun, S. S. Lim, Y. M. Lam, M. Grätzel, S. Mhaisalkar, T. C. Sum, *Science* **2013**, *342*, 344.
- [7] W. Rehman, D. P. McMeekin, J. B. Patel, R. L. Milot, M. B. Johnston, H. J. Snaith, L. M. Herz, *Energy Environ. Sci.* **2017**, *10*, 361.
- [8] A. Rajagopal, R. J. Stoddard, H. W. Hillhouse, A. K.-Y. Jen, *J. Mater. Chem. A* **2019**, *7*, 16285.
- [9] W. Shockley, H. J. Queisser, *J. Appl. Phys.* **1961**, *32*, 510.
- [10] K. A. Bush, A. F. Palmstrom, Z. J. Yu, M. Boccard, R. Cheacharoen, J. P. Mailoa, D. P. McMeekin, R. L. Z. Hoyer, C. D. Bailie, T. Leijtens, I. M. Peters, M. C. Minichetti, N. Rolston, R. Prasanna, S. Sofia, D. Harwood, W. Ma, F. Moghadam, H. J. Snaith, T. Buonassisi, Z. C. Holman, S. F. Bent, M. D. McGehee, *Nat. Energy* **2017**, *2*, 17009.
- [11] T. Leijtens, K. A. Bush, R. Prasanna, M. D. McGehee, *Nat. Energy* **2018**, *3*, 828.
- [12] G. E. Eperon, T. Leijtens, K. A. Bush, R. Prasanna, T. Green, J. T.-W. Wang, D. P. McMeekin, G. Volonakis, R. L. Milot, R. May, A. Palmstrom, D. J. Slotcavage, R. A. Belisle, J. B. Patel, E. S. Parrott, R. J. Sutton, W. Ma, F. Moghadam, B. Conings, A. Babayigit, H.-G. Boyen, S. Bent, F. Giustino, L. M. Herz, M. B. Johnston, M. D. McGehee, H. J. Snaith, *Science* **2016**, *354*, 861.
- [13] J. H. Noh, S. H. Im, J. H. Heo, T. N. Mandal, S. Seok, *Nano Lett.* **2013**, *13*, 1764.
- [14] L. Protesescu, S. Yakunin, M. I. Bodnarchuk, F. Krieg, R. Caputo, C. H. Hendon, R. X. Yang, A. Walsh, M. V. Kovalenko, *Nano Lett.* **2015**, *15*, 3692.
- [15] K. J. Savill, A. M. Ulatowski, L. M. Herz, *ACS Energy Lett.* **2021**, *6*, 2413.
- [16] E. S. Parrott, T. Green, R. L. Milot, M. B. Johnston, H. J. Snaith, L. M. Herz, *Adv. Funct. Mater.* **2018**, *28*, 1802803.
- [17] S. Gu, R. Lin, Q. Han, Y. Gao, H. Tan, J. Zhu, *Adv. Mater.* **2020**, *32*, 1907392.
- [18] T. Leijtens, R. Prasanna, A. Gold-Parker, M. F. Toney, M. D. McGehee, *ACS Energy Lett.* **2017**, *2*, 2159.
- [19] C. Wang, Z. Song, C. Li, D. Zhao, Y. Yan, *Adv. Funct. Mater.* **2019**, *29*, 1808801.
- [20] L. Lanzetta, T. Webb, N. Zibouche, X. Liang, D. Ding, G. Min, R. J. E. Westbrook, B. Gaggio, T. J. Macdonald, M. S. Islam, S. A. Haque, *Nat. Commun.* **2021**, *12*, 2853.
- [21] L. Lanzetta, N. Aristidou, S. A. Haque, *J. Phys. Chem. Lett.* **2020**, *11*, 574.
- [22] H. Yao, F. Zhou, Z. Li, Z. Ci, L. Ding, Z. Jin, *Adv. Sci.* **2020**, *7*, 1903540.
- [23] M. H. Kumar, S. Dharani, W. L. Leong, P. P. Boix, R. R. Prabhakar, T. Baikie, C. Shi, H. Ding, R. Ramesh, M. Asta, M. Graetzel, S. G. Mhaisalkar, N. Mathews, *Adv. Mater.* **2014**, *26*, 7122.

- [24] K. P. Marshall, M. Walker, R. I. Walton, R. A. Hatton, *Nat. Energy* **2016**, *1*, 16178.
- [25] D. Ricciarelli, D. Meggiolaro, F. Ambrosio, F. De Angelis, *ACS Energy Lett.* **2020**, *5*, 2787.
- [26] D. Meggiolaro, D. Ricciarelli, A. A. Alasmari, F. A. S. Alasmay, F. De Angelis, *J. Phys. Chem. Lett.* **2020**, *11*, 3546.
- [27] N. K. Noel, S. D. Stranks, A. Abate, C. Wehrenfennig, S. Guarnera, A.-A. Haghighirad, A. Sadhanala, G. E. Eperon, S. K. Pathak, M. B. Johnston, A. Petrozza, L. M. Herz, H. J. Snaith, *Energy Environ. Sci.* **2014**, *7*, 3061.
- [28] Y. Takahashi, R. Obara, Z. Z. Lin, Y. Takahashi, T. Naito, T. Inabe, S. Ishibashi, K. Terakura, *Dalton Trans.* **2011**, *40*, 5563.
- [29] G. Nasti, A. Abate, *Adv. Energy Mater.* **2020**, *10*, 1902467.
- [30] R. L. Milot, M. T. Klug, C. L. Davies, Z. Wang, H. Kraus, H. J. Snaith, M. B. Johnston, L. M. Herz, *Adv. Mater.* **2018**, *30*, 1804506.
- [31] K. J. Savill, A. M. Ulatowski, M. D. Farrar, M. B. Johnston, H. J. Snaith, L. M. Herz, *Adv. Funct. Mater.* **2020**, *30*, 2005594.
- [32] G. Li, Z. Su, M. Li, F. Yang, M. H. Aldamasy, J. Pascual, F. Yang, H. Liu, W. Zuo, D. Di Girolamo, Z. Iqbal, G. Nasti, A. Dallmann, X. Gao, Z. Wang, M. Saliba, A. Abate, *Adv. Energy Mater.* **2021**, *11*, 2101539.
- [33] X. Meng, Y. Wang, J. Lin, X. Liu, X. He, J. Barbaud, T. Wu, T. Noda, X. Yang, L. Han, *Joule* **2020**, *4*, 902.
- [34] L. He, H. Gu, X. Liu, P. Li, Y. Dang, C. Liang, L. K. Ono, Y. Qi, X. Tao, *Matter* **2020**, *2*, 167.
- [35] G. Liu, C. Liu, Z. Lin, J. Yang, Z. Huang, L. Tan, Y. Chen, *ACS Appl. Mater. Interfaces* **2020**, *12*, 14049.
- [36] L. M. Herz, *ACS Energy Lett.* **2017**, *2*, 1539.
- [37] A. M. Ulatowski, L. M. Herz, M. B. Johnston, *J. Infrared Millim. Terahertz Waves* **2020**, *41*, 1431.
- [38] C. C. Stoumpos, C. D. Malliakas, M. G. Kanatzidis, *Inorg. Chem.* **2013**, *52*, 9019.
- [39] R. L. Milot, G. E. Eperon, T. Green, H. J. Snaith, M. B. Johnston, L. M. Herz, *J. Phys. Chem. Lett.* **2016**, *7*, 4178.
- [40] E. Burstein, *Phys. Rev.* **1954**, *93*, 632.
- [41] T. S. Moss, *Proc. Phys. Soc. Sect. B* **1954**, *67*, 775.
- [42] T. Handa, T. Yamada, H. Kubota, S. Ise, Y. Miyamoto, Y. Kanemitsu, *J. Phys. Chem. C* **2017**, *121*, 16158.
- [43] A. Chernikov, A. M. Van Der Zande, H. M. Hill, A. F. Rigosi, A. Velauthapillai, J. Hone, T. F. Heinz, *Phys. Rev. Lett.* **2015**, *115*, 126802.
- [44] R. J. Elliott, *Phys. Rev.* **1957**, *108*, 1384.
- [45] J. M. Ball, A. Petrozza, *Nat. Energy* **2016**, *1*, 16149.
- [46] X. Qiu, B. Cao, S. Yuan, X. Chen, Z. Qiu, Y. Jiang, Q. Ye, H. Wang, H. Zeng, J. Liu, M. G. Kanatzidis, *Sol. Energy Mater. Sol. Cells* **2017**, *159*, 227.
- [47] A. G. Kontos, A. Kaltzoglou, E. Siranidi, D. Palles, G. K. Angeli, M. K. Arfanis, V. Psycharis, Y. S. Raptis, E. I. Kamitsos, P. N. Trikalitis, C. C. Stoumpos, M. G. Kanatzidis, P. Falaras, *Inorg. Chem.* **2017**, *56*, 84.
- [48] A. Kaltzoglou, M. Antoniadou, A. G. Kontos, C. C. Stoumpos, D. Perganti, E. Siranidi, V. Raptis, K. Trohidou, V. Psycharis, M. G. Kanatzidis, P. Falaras, *J. Phys. Chem. C* **2016**, *120*, 11777.
- [49] Y. El Ajjouri, F. Locardi, M. C. Gélvez-Rueda, M. Prato, M. Sessolo, M. Ferretti, F. C. Grozema, F. Palazon, H. J. Bolink, *Energy Technol.* **2020**, *8*, 1900788.
- [50] L. E. Mundt, J. Tong, A. F. Palmstrom, S. P. Dunfield, K. Zhu, J. J. Berry, L. T. Schelhas, E. L. Ratcliff, *ACS Energy Lett.* **2020**, *5*, 3344.
- [51] D. Meggiolaro, S. G. Motti, E. Mosconi, A. J. Barker, J. Ball, C. Andrea Riccardo Perini, F. Deschler, A. Petrozza, F. De Angelis, *Energy Environ. Sci.* **2018**, *11*, 702.
- [52] H. Jin, E. Debroye, M. Keshavarz, I. G. Scheblykin, M. B. J. Roeloffs, J. Hofkens, J. A. Steele, *Mater. Horiz.* **2020**, *7*, 397.
- [53] S. G. Motti, D. Meggiolaro, S. Martani, R. Sorrentino, A. J. Barker, F. De Angelis, A. Petrozza, *Adv. Mater.* **2019**, *31*, 1901183.
- [54] A. R. Bowman, M. T. Klug, T. A. S. Doherty, M. D. Farrar, S. P. Senanayak, B. Wenger, G. Divitini, E. P. Booker, Z. Andaji-Garmaroudi, S. Macpherson, E. Ruggeri, H. Sirringhaus, H. J. Snaith, S. D. Stranks, *ACS Energy Lett.* **2019**, *4*, 2301.
- [55] J. Chen, N. G. Park, *Adv. Mater.* **2019**, *31*, 1803019.
- [56] P. Xu, H. He, J. Ding, P. Wang, H. Piao, J. Bao, W. Zhang, X. Wu, L. Xu, P. Lin, X. Yu, C. Cui, *ACS Appl. Energy Mater.* **2021**, *4*, 10921.
- [57] F. Gu, S. F. Wang, C. F. Song, M. K. Lü, Y. X. Qi, G. J. Zhou, D. Xu, D. R. Yuan, *Chem. Phys. Lett.* **2003**, *372*, 451.
- [58] L. Xiong, Y. Guo, J. Wen, H. Liu, G. Yang, P. Qin, G. Fang, *Adv. Funct. Mater.* **2018**, *28*, 1802757.
- [59] D. Liu, Y. Wang, H. Xu, H. Zheng, T. Zhang, P. Zhang, F. Wang, J. Wu, Z. Wang, Z. Chen, S. Li, *Sol. RRL* **2019**, *3*, 1800292.
- [60] J. Xie, K. Huang, X. Yu, Z. Yang, K. Xiao, Y. Qiang, X. Zhu, L. Xu, P. Wang, C. Cui, D. Yang, *ACS Nano* **2017**, *11*, 9176.
- [61] K. G. Godinho, A. Walsh, G. W. Watson, *J. Phys. Chem. C* **2009**, *113*, 439.
- [62] D. J. Kubicki, D. Prochowicz, E. Salager, A. Rakhmatullin, C. P. Grey, L. Emsley, S. D. Stranks, *J. Am. Chem. Soc.* **2020**, *142*, 7813.